Investigation of the Combined Efficiency of a Solar/Gas Hybrid Water Heating System

Saroj KARKI [(a)], Karl R. HAAPALA[(a)] and Brian M. FRONK [(a) (b)]

[(a)] School of Mechanical, Industrial and Manufacturing Engineering
Oregon State University
Corvallis, OR 97331 USA

[(b)] Corresponding author: E-mail:brian.fronk@oregonstate.edu; Phone: +1-541-737-3952

Abstract

In climate regions with large seasonal variations in solar radiation, such as the Pacific Northwest of the United States, a solar thermal energy collector might not economically satisfy year-round domestic water heating demands, requiring an auxiliary unit, such as a natural gas-fired water heater. Previous studies have shown that the burner efficiency of a gas-fired water heater varies depending on the log-mean temperature difference between the cold fluid (water) and the hot fluid (combustion gases). In a solar/gas hybrid water heating system where solar collectors are used in conjunction with a gas-fired heater, the partial heating of water provided by solar input reduces the log-mean temperature difference value for the gas heater, reducing the efficiency of the gas burner. Since this efficiency reduction varies depending on the amount of pre-heating provided by solar energy input, it is difficult to accurately predict the actual cost and energy savings offered by solar/gas hybrid water heaters in different climate scenarios. Hence, to predict the actual energy and cost savings under various design conditions, the performance of solar/gas hybrid systems must be better understood.

The purpose of this work is to experimentally determine the thermal performance of a solar/gas water hybrid water heating system with a 6.44 m^2 flat plate solar collector array and a 22.3 kW natural gas burner in Corvallis, Oregon. Under different temperature lifts and solar insolation values, the system was operated at three different modes of heating: solar, gas, and combined solar/gas mode. The overall system thermal efficiency value for each mode is calculated. The efficiency of the solar collector heating system was found to be 41.97%, 39.82%, and 35.05% at initial water temperature of 20, 30, and 51.5 °C, respectively. For initial water temperatures of 20, 30, and 51.5 °C, the efficiency of the gas burner was found to be 69.2%, 66.4%, and 65.5% at the HHV, and 76.7%, 73.6%, and 72.6% at the LHV of natural gas, respectively. In the combined solar/gas heating mode, the efficiency of the gas burner decreased with increasing solar fraction. For solar fractions of 4.93%, 9.40%, 11.39%, and 14.27%, the efficiency of the gas burner in terms of the HHV of natural gas was found to be of 69.08%, 66.80%, 66.17%, and 65.18%, respectively. Based on the experimental results, a configuration that would provide higher overall system efficiency for combined solar/gas heating is suggested.

Keywords: Solar thermal; natural gas; water heating

1. Introduction

Water heating accounts for approximately 18% of the total residential energy consumption in the United States [1]. Historically and currently, the water heater market in the US has been dominated by gas-fired and electric resistance storage type and tankless water heaters [2]. A breakdown of US residential water heating energy use indicates that approximately 48% of households use natural gas, while approximately 45% use electricity for water heating [3]. With the increasing concerns of carbon emissions and other environmental impacts associated with the extraction and use of fossil fuels, there is interest in developing renewable energy sources for domestic water heating.

Solar thermal water heating systems (STWHS) are a simple and cost-effective renewable technology for harnessing the sun's energy to generate hot water. The main components of a typical STWHS are a solar collector, a hot water storage tank, and a control system. The operating principle is that the solar collector absorbs the incident solar radiation and transfers the energy to a working fluid (water or solar fluid) flowing inside the collector tubes. The heated working fluid can be used either directly in the form of hot water, or to charge a thermal energy storage tank from where energy can be drawn for use later. A flat-plate collector (FPC) is the most common type of solar collector used for harvesting solar energy at relatively low fluid temperatures [4], and has seen commercial application around the world. It consists of a selective flat plate absorber covered by a transparent glass or plastic cover (glazing) to reduce heat loss from the top surface, tubes to circulate the heat transfer fluid within the body of the collector, and insulation to minimize heat losses from the sides and bottom surface of the absorber plate [4].

The percentage of water heating energy required by a household that is provided by the solar collectors is quantified in terms of solar fraction. For a given collector area, solar fraction varies primarily with the amount of incident solar radiation [5]. Due to the diurnal and seasonal variation of available solar energy, an auxiliary heating source is generally necessary to provide backup heating whenever solar energy fails to meet the energy demand [4]. Electric resistance heaters are the most commonly used backup energy source.

Numerous experimental studies have been carried out to analyze the thermal performance of FPC solar water heating systems under steady-state and quasi-dynamic test conditions following EN 12975-2 [6] and ASHRAE 93-2003 [7] standards, among others. For example, Rojas et al. [8] and

Anderson et al. [9] studied the thermal performance of FPCs under steady-state conditions following the ASHRAE standard, while Zambolin and Del Col [10] and Rodriguez-Hidalgo et al. [11] measured the thermal efficiency of FPCs under steady-stated and quasi-dynamic state following the EN standard. However, these standards require experimental data to be collected under prescribed environmental conditions which may not necessarily represent the actual operating conditions experienced by the solar collectors. For example, a minimum solar radiation of 790 and 700 W m^{-2} is required by the ASHRAE 93 and EN 12975-2 standards, respectively, to conduct the thermal efficiency tests [8]. In practice, however, solar radiation values fluctuate depending on the weather conditions, location, season, and time of the day. Furthermore, these standards are a test of the solar collector efficiency only, and do not account for the efficiency of an auxiliary heating system that would be required in many climate regions. Some researchers have performed experimental studies of FPCs under real weather conditions. Rodriguez-Hidalgo et al. [12] carried out an experimental study to evaluate the performance of a 50 m^2 FPC for domestic hot water heating and cooling application in Madrid, Spain. Using the collected data, they quantified the sensitivity of instantaneous thermal performance of solar collectors to the following factors: wind thermal loss, collector aging, thermal capacitance, irradiance incidence angle, and radiation loss.

Michaelides and Eleftheriou [13] studied the thermal performance of a solar water heating system utilizing a 3 m^2 FPC and a 68 L storage tank under real weather conditions in Cyprus over a two-year period. They found that the annual average daily performance of the system was relatively insensitive to solar radiation fluctuations ranging from 800 to 1100 W m^{-2}. The effect of fluctuating solar radiation was pronounced only in the instantaneous energy and efficiency values. Ayompe and Duffy [14] experimentally measured the thermal performance of a solar water heating system with 4 m^2 FPCs located in Dublin, Ireland and reported an annual average daily solar fraction of 32.2%, collector efficiency of 45.6%, and overall system efficiency of 37.8%. In all of the above-mentioned studies, an electric immersion heater was used as the auxiliary energy source. Electric resistance heaters are ~100% efficient [15], meaning all the input electric energy is converted into heat and supplied to the water. This conversion efficiency is not dependent on the temperature of the heated water. Since the efficiency of electric heating is constant, it is straightforward to predict the cost and energy of the required auxiliary energy when the solar fraction is known. However, with natural gas-fired water heating systems, the efficiency varies depending on the amount of

heat transferred in the heat exchanger, which is directly impacted by the temperature difference between the cold fluid (water) and the hot fluid (combustion gases).

Presently, the cost of natural gas in the US is below the cost of electricity on a kWh-to-kWh basis [16], making natural gas backup an attractive option in terms of auxiliary energy cost. Furthermore, depending on the feedstock energy source for generating electricity, there may be advantages from carbon emissions and primary energy consumption perspectives in obtaining auxiliary heating directly with gas [17]. However, previous studies [18–20] have shown that the efficiency of gas-fired water heaters decreases with increasing inlet water temperature. With an increase in inlet water temperature, the temperature difference between the combustion gases and tank water decreases, reducing the heat transfer rate. In a solar/gas hybrid water heating system where the solar collector is used in conjunction with a gas-fired heater, the partial heating of process fluid provided by solar input reduces the log-mean temperature difference (LMTD) value for the gas heater, reducing the efficiency of the gas burner. Therefore, lower overall system efficiency than expected may be observed while running a solar/gas hybrid water heating system in a combined solar/gas mode. Since this efficiency varies depending on the amount of pre-heating provided by solar input, it is challenging to accurately predict the actual cost and energy savings offered by a solar/gas water heater.

Hence, to predict the actual energy and cost savings under various design conditions, the performance of solar/gas hybrid systems must be better understood. Therefore, the objective of this work is to experimentally determine the thermal performance of a commercial solar/gas water hybrid water heating system with a 6.44 m^2 flat plate solar collector array and a 22.3 kW natural gas burner under actual operating conditions. Expanding from prior work by Karki et al. [21], the system was operated at three different modes of heating: solar only, gas only, and combined solar/gas modes for different temperature lifts and solar insolation values. Efficiency values for each mode were calculated. Based on the experimental efficiency results, potential configurations that would provide optimal efficiency for the combined solar/gas mode of heating are suggested.

2. Experimental Setup and Data Reduction Methods

2.1. Experimental Setup

An active closed loop hybrid solar thermal water heating system (STWHS) installed on a campus building at Oregon State University in Corvallis, Oregon (44.56° N, 123.27° W), provides the basis for this experimental study. The STWHS consists of 6.44 m^2 FPC array, a 265 L hot water storage tank, a pump with maximum flow rate of 0.63 L/sec, and a commercial control unit. A schematic diagram of the experimental setup is shown in Figure 1, and photographs of the key system components in Figure 2.

The collector array consists of three Schüco Slim V Plus FPCs connected in series (Figure 2a); each FPC has a gross area of 2.32 m^2 and an aperture area of 2.148 m^2. The collectors face south and are inclined at 45 degrees. As stated by the manufacturer, each collector has an optical efficiency, or "zero loss efficiency," rating of 76.7%. The collector heat loss coefficient values, k_1 and k_2, are defined to be 3.71 and 0.016 W m^{-2} K^{-1}, respectively. The absorber plate is made up of copper tubes covered with a high selectivity coating that has short-wave absorptivity of 95% and long wave emissivity of 5%. Each collector is covered by a 4-mm thick low iron glazing of 91% transmittance. The sides and bottom surface of the collectors are insulated with mineral wool insulation (20 mm thick). The maximum operating temperature and pressure of the collectors are 120 °C and 10 bars, respectively.

The storage tank is a Schüco S WW 70-1GPN model (Figure 2b), constructed of stainless steel. It is equipped with an auxiliary 22.27 kW natural gas burner, which has a specified efficiency rating of 80% based on natural gas lower heating value. The tank contains an immersed solar heating coil that allows heat transfer between the solar fluid and potable water. The solar coil has a heat transfer surface area of 1.31 m^2. Non-CFC foam insulation (50.8 mm thickness) covers the sides and the top of the tank.

A solution of water and propylene glycol (40% propylene glycol by mass) is used as the heat transfer fluid to provide freeze protection during colder months. As shown in the schematic in Figure 1, the glycol water mixture is pumped through the FPC array, where it absorbs the incoming solar energy. The hot glycol water mixture then passes through the solar heating coils inside the storage tank where it exchanges heat with the tank water.

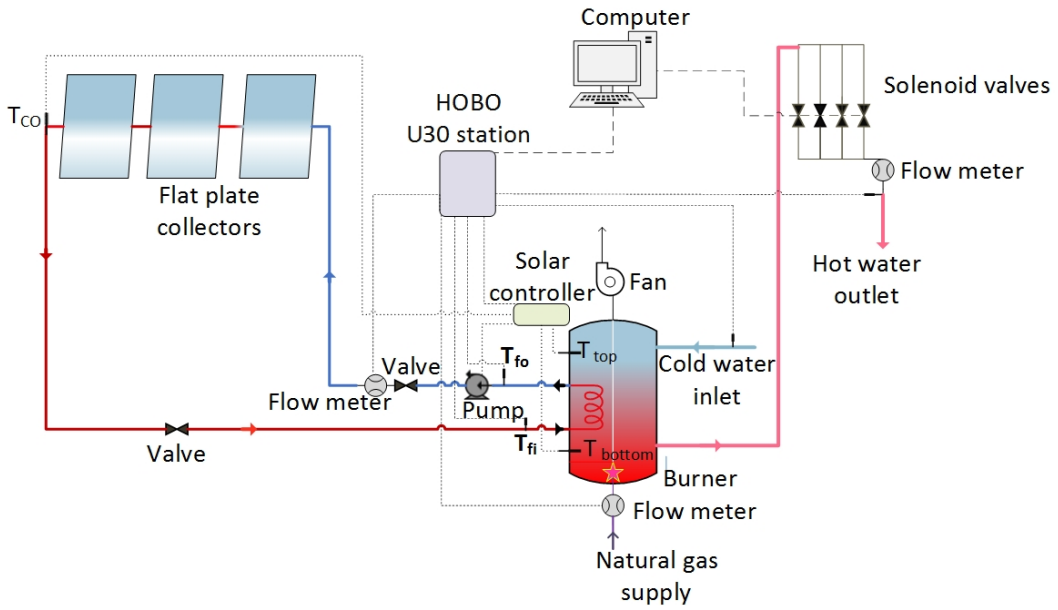

Figure 1: Schematic diagram of the experimental setup

The natural gas burner is used to raise the tank temperature whenever the solar energy is insufficient to heat the tank to the required temperature of 60 °C. The hot water draw-off system consists of four solenoid valves that run parallel to each other, each with a different flow restrictor (Figure 2c). The array of valves can be actuated in different combinations to achieve 15 distinct flowrates ranging from 0.94 to 16 liters per minute. This arrangement provides the capability to simulate actual residential hot water draws. The opening and closing operation of the valves is controlled by a program written in LabVIEW software.

2.2. Instrumentation

The STWHS is equipped with a HOBO U30 station for monitoring and data logging sensors at a specific time interval. The station is configured with 14 data channels via a plug-in modular connector. The following system parameters are data logged: global solar radiation, collector outlet temperature, temperatures of the glycol water mixture at the inlet and outlet of the solar coil, water temperatures at the top and bottom of the storage tank, cold water (building) inlet temperature, delivered hot water exit temperature, volumetric flow rate of the circulating glycol water mixture, and volumetric flow rate of natural gas.

The operation of the solar glycol loop is controlled by a Schüco IM TH3001 DeltaSol solar controller (Figure 2d). The controller has a semiconductor relay which controls the operation of

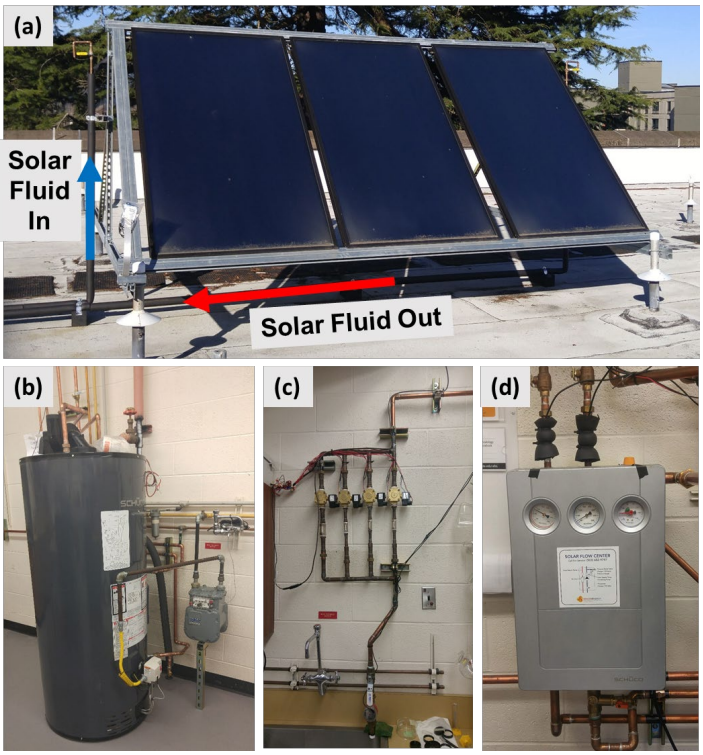

Figure 2: Photograph of the experimental setup showing (a) flat plate collectors, (b) storage tank with gas-fired backup, (c) solenoid valve array for simulating hot water draws and (d) solar pump controller

the solar pump based on the temperature difference between the solar fluid exiting the collector and water inside the storage tank. Three Pt1000 temperature sensors are connected to the solar controller to measure collector temperature, temperature of water at the top of the storage tank, and temperature of water at the bottom of the storage tank. A summary of all instruments data logged is provided in Table 1.

The circulating water glycol loop has a flow sensor that emits one pulse per gallon flow of glycol. Each pulse is sent to and recorded using the HOBO unit. Similarly, the AC-250 diaphragm gas meter is connected to the HOBO unit by an S-UCC-M006 pulse input adaptor. For each cubic foot of natural gas consumed, a pulse is sent to and recorded by the HOBO unit.

Table 1: Summary of measuring instruments.

Parameter measured	Sensor type	Sensor make/model	Measurement uncertainty
Glycol supply temperature	Thermistor	METRIMA SVM TDA	±0.15% (±0.02 °C)
Glycol return temperature	Thermistor	METRIMA SVM TDA	±0.15% (±0.02 °C)
Tank water inlet temperature	Thermistor	ONSET S-TMB-M002	±0.2 °C for 0 to 50 °C
Hot water exit temperature	Thermistor	ONSET S-TMB-M002	±0.2 °C for 0 to 50 °C
Solar radiation	Pyranometer	S-LIB-M003	±5% (±10 W m^{-2})
Volumetric flow rate of glycol	-	METRIMA SVM F2	±0.35%
Natural gas flow rate	Diaphragm meter	AC-250	-

All sensors were sampled at a 10-second interval. Physical properties of the fluid, such as density and specific heat capacity, were calculated at the corresponding fluid temperature. Energy and system efficiency values were calculated using the instantaneous experimental data collected under the outdoor conditions. To smooth the short-term fluctuations of the collected data, a 25-minute rolling average of the measured values was used in the data analysis.

3. Performance Metrics

As noted above, system performance data were collected for three different modes of operation: solar energy mode, natural gas energy mode, and hybrid (solar and natural gas) mode. The following performance metrics were calculated: energy delivered to the water tank, solar fraction, collector system efficiency, gas burner efficiency, and hybrid system efficiency, as described below.

3.1. Solar Mode of Operation

In the solar mode of operation, water inside the storage tank is heated using solar energy only. The rate of useful energy delivered by the solar fluid to the storage tank is calculated as [4] Eq. (1):

$$\dot{Q}_d = \dot{m} c_{p,g} (T_{fi} - T_{fo}) \quad (1)$$

The collector system efficiency is calculated as shown in Eq. (2) and defined in [4]. This value includes not only the efficiency of the collector itself, but also heat losses between the collector and storage tank, and the effectiveness of the solar heat exchanger located inside the storage tank.

$$\eta_s = \frac{\dot{m} c_{p,g} (T_{fo} - T_{fi})}{A_c G_t} \quad (2)$$

3.2. Natural Gas Mode of Operation

In this mode of operation, water inside the tank is heated using natural gas energy only. As reported by Aldrich [22], the burner efficiency (given by Eq. (3)) is defined as the ratio of energy gained by the storage tank to the total natural gas energy supplied.

$$\eta_{burner} = \frac{m c_{p,w} (T_{ini} - T_{fin})}{V_{gas} * HV} \quad (3)$$

In this study, efficiency values are presented for both the higher and lower heating values of natural gas.

3.3. Hybrid Mode of Operation

In the hybrid mode of operation, water inside the storage tank is heated using both solar and natural gas energy. Solar fraction is defined as the ratio of the amount of energy provided by solar collector to the total energy required for water heating. It is calculated as defined in [5], shown in Eq. (4):

$$f = \frac{Q_{solar}}{Q_{solar} + Q_{auxiliary}} \quad (4)$$

The rate of energy provided by the solar collector was calculated using Eq. (1). The total solar heating time is then multiplied by the energy rate to calculate the total amount of solar energy delivered. The amount of auxiliary energy provided by gas heater was calculated by subtracting the energy delivered by the solar collector from the calculated total energy gained by the water during heating.

3.4. Uncertainty Analysis

Experimental errors are unwanted but an inherent problem in an experimental data collection process. Experimental uncertainty due to calibration error, data recording error, and unsuitable instrument error might lead to misleading results. To reduce the effect of such experimental errors, each experiment was repeated four times. The uncertainty of all calculated values is reported following NIST guidelines [23]. In many cases, the desired result of a physical experiment is not directly measured but is derived using one or more directly measured variables. For example, the efficiency of the collector heating system, as shown in Eq. (2), is not directly measured but is derived using directly measured values of mass flow rate, glycol inlet and exit temperature, and solar radiation. If a physical quantity Y is a function of n variables, $X_1, X_2, \ldots, X_n$ that are measured separately, the value of indirectly measured quantity Y can be calculated as specified in [23] and shown in Eq. (5):

$$Y = f(X_1, X_2, \ldots X_n) \tag{5}$$

Assuming the measured variables (X_1, $X_2 \ldots$, X_n) as uncorrelated and random, the combined uncertainty of the derived quantity Y can be calculated as specified in Eq. (6):

$$U_Y = \sqrt{\sum_{i=0}^{n} \left(\frac{\partial y}{\partial x_i}\right)^2 U_{X_i}^{\ 2}} \tag{6}$$

where $\left(\frac{\partial y}{\partial x_i}\right)$ represents the partial derivative of the function $f(X_1, X_2, \ldots X_n)$ with respect to the variable X_i and U_{X_i} represents the standard deviation of the measured variable X_i. Using this uncertainty propagation method, the uncertainty of derived variables, efficiency of collector, and gas-heater efficiency are calculated using built-in capabilities of *Engineering Equation Solver* software [24] and reported in the following sections.

4. Results and Discussions

4.1. Solar Only Heating Mode

The efficiency of the solar collector heating system was measured at three initial tank temperatures of 20, 30, and 51.5 °C. The final temperature in all cases was 60 °C, as this is the default setting

on most commercial systems in the United States. These three cases are intended to simulate system performance for a full tank discharge and reheat (ΔT = 40 °C), recovery from a larger water draw (ΔT = 30 °C), and recovery from a small draw or standby losses (ΔT = 8.5 °C). A summary of the results of the solar tests is shown in Table 2. Using the uncertainty propagation discussed above, the maximum uncertainty in the calculated efficiency was ±0.09%.

Table 2: Summary of solar tests

Initial Tank Temperature (±0.2 °C)	Range of Incident Solar Flux (±10 W m^{-2})	Number of Experiments Run	Range of Time to Heat Tank (hrs.)	Range of Overall Efficiency (%)
20.0	780 to 860	4	5.07 to 6.45	41.8 to 43.2
30.0	916 to 935	4	3.72 to 4.53	38.9 to 40.5
51.5	862 to 926	4	1.15 to 2.45	34.9 to 35.2

Figure 3 shows the solar radiation, mass flow rate of glycol, temperature difference between the glycol inlet and outlet temperature in the in-tank solar coil, tank water temperature, and collector heating system efficiency curve for a typical summer day (8/22/2017) with the storage tank initially at 20 °C. Data is presented with a 25-minute rolling average applied. In this experimental run, it took approximately 6.32 hours to heat the tank water to the required temperature of 60 °C. The measured average solar radiation for the period of the experiment was 780 W m^{-2}. Depending on the intensity of solar radiation and the temperature of the water glycol fluid, the solar fluid mass flow rate varied between 42.5 and 63.7 g s^{-1}, with an average mass flow rate of 58.7 g s^{-1}. The average temperature difference between the glycol water mixture at the inlet and outlet of the tank solar coil was 10.15 °C. The average efficiency of the collector heating system (defined by Eq. (2)) was found to be 41.83 %. The average efficiency is defined as the sum of all instantaneous (at every 10-second interval) efficiencies divided by the total number of data points during the solar heating time.

During the first few minutes of the test, the pump circulated the stagnant glycol water mixture which had been preheated in the collector loop to a high temperature to the water storage tank. This resulted in a larger than expected solar fluid temperature difference (delta t) in the first few minutes of the test and the unusual spike at the beginning of the efficiency curve shown in Figure 3. Once the stagnant glycol water mixture was fully circulated, the solar fluid temperature difference value became stable and representative of the instantaneous solar radiation.

According to Eq. (2), for a constant mass flow rate, instantaneous efficiency of a collector heating system depends on the solar fluid temperature difference and solar radiation. The effect of solar radiation on the collector system efficiency curve can be seen in Figure 3. As expected, as the solar radiation value decreases, the collector system efficiency also decreases.

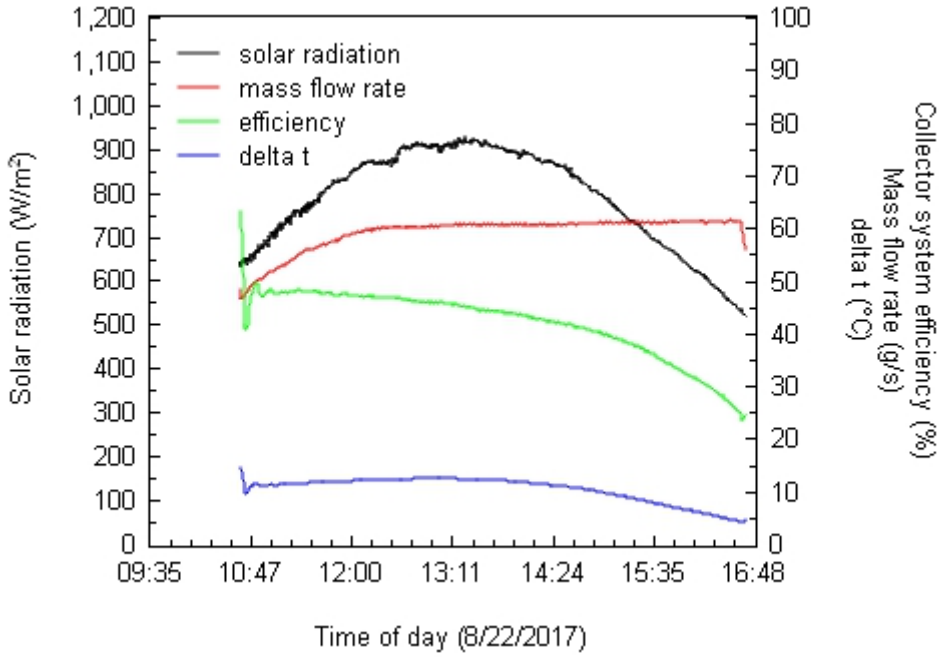

Figure 3: Collected sensor data and calculated efficiency values for a typical summer day (25-minute rolling average)

For steady-state operating conditions, the useful energy collected by an FPC under a near-normal incidence angle of solar radiation is calculated using the Hottel-Whillier-Bliss equation as reported by Duffie and Beckman [4] and shown in Eq. (7):

$$Q_u = F_R A_c [G_t(\tau\alpha) - U_L(T_i - T_a)] \qquad (7)$$

As per Eq. (7), an FPC would collect the maximum possible energy if the temperature of the fluid entering the collector (T_i) were always at a minimum possible temperature, or in other words, if the term ($T_i - T_a$) in Eq. (7) was close to zero. However, the temperature of the fluid entering the collector is not a design variable and cannot be controlled [25]. If we assume negligible piping heat losses and efficient heat exchange between the solar fluid and water, the collector fluid inlet temperature will be nearly equal to the storage tank temperature [25]. As the collector fluid inlet temperature increases, the collector heat loss value increases and, hence, less energy is collected.

Moreover, in real life operating conditions, we cannot assume a constant heat transfer rate between the solar fluid and the tank water will occur. With an increase in tank water temperature and an approximately constant collector outlet temperature, the LMTD between the solar fluid and tank water decreases, reducing the rate of heat exchange between solar fluid and tank water. As a result, the efficiency of the solar heat exchanger decreases. For these two reasons, the efficiency of the solar collector heating decreases with an increase in tank water temperature. This efficiency reduction was experimentally observed.

Figure 4 shows the average daily efficiency of the solar collector heating system for all four tests at different initial tank water temperatures and a final tank temperature of 60 °C. Taking into consideration that the average collector efficiency does not change significantly with change in solar radiation for a solar radiation range of 800 to 1100 W m^{-2}, it is seen that the efficiency of the collector heating system decreased with increase in the initial tank water temperature. The efficiency of the collector heating system in completely heating water to 60 °C was found to be 42.01±0.09%, 39.82±0.08%, and 35.05±0.07% at initial water temperatures of 20±0.2, 30±0.2, and 51.5±0.2 °C, respectively. The reduction in efficiency with increasing inlet water temperature was expected and agrees with the trends cited in literature, such as those reported by You and Hu [26] and Celuppi et al. [27].

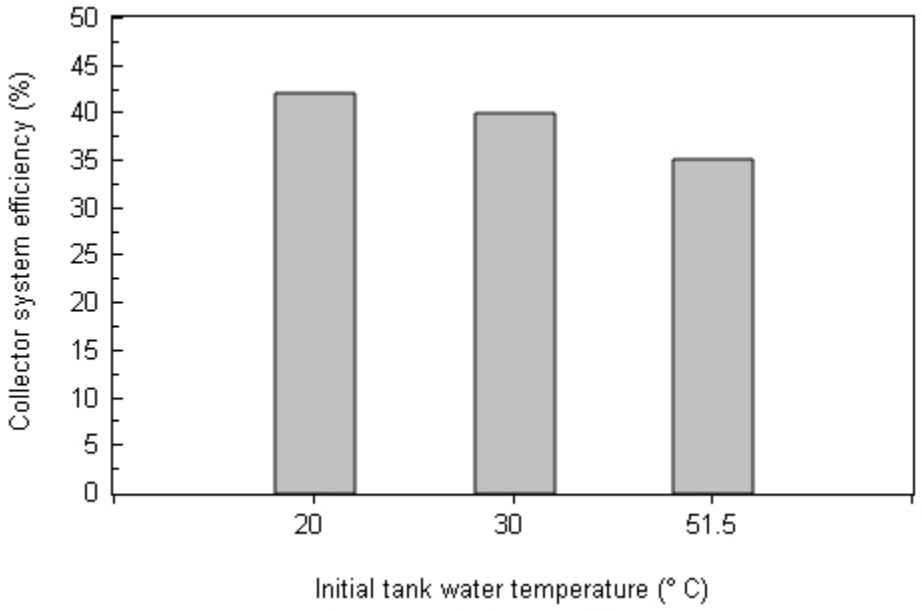

Figure 4: Collector system efficiency at different tank water temperatures

4.2. Natural Gas Burner Efficiency at Different Starting Temperatures

Using natural gas only, the tank water was heated to a final temperature of 60 ± 0.2 °C from three different inlet temperatures. Using Eq. (3), the efficiency of the gas burner was calculated and reported in terms of higher heating value (HHV) and lower heating value (LHV) of natural gas. The higher and lower heating values of natural gas used in the calculation were 52.225 and 47.141 MJ kg^{-1}, respectively [28]. The efficiency of the gas burner was found to be 69.20±0.14%, 66.41±0.13%, and 65.51±0.12% for HHV and 76.15±0.15%, 73.59±0.14%, and 72.60±0.14% for LHV for initial tank water temperature of 20, 30, and 51.5 ±0.2 °C, respectively. Results are summarized graphically in Figure 5.

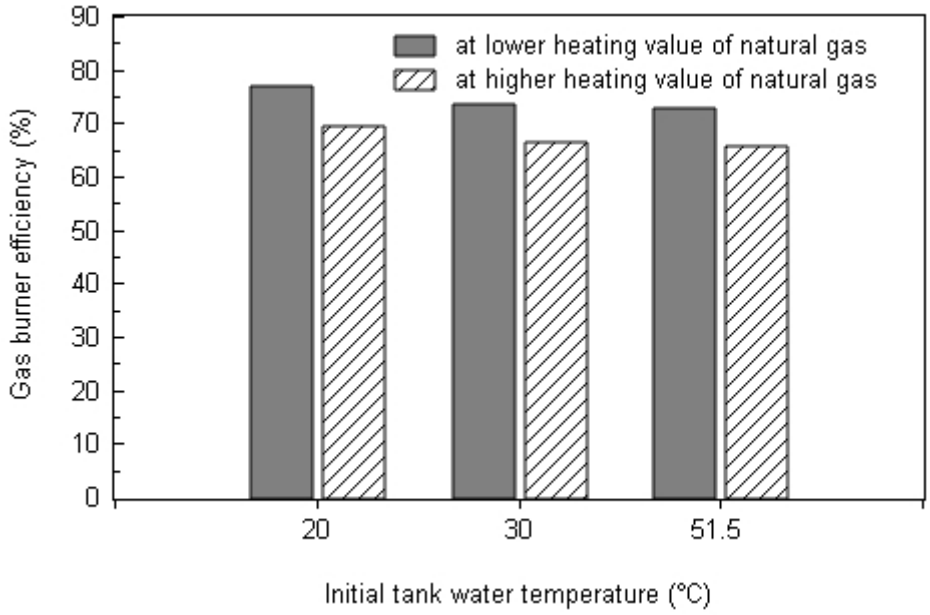

Figure 5: Natural gas burner efficiency for three different tank water temperatures

It is seen that the efficiency of the gas burner is highest at an initial temperature of 20 °C and, as expected, decreases with increasing initial tank water temperature. As the tank water temperature increases, the temperature difference between the cold side (tank water) inlet temperature and hot side (combustion gas) exit temperature decreases. As a result, the temperature driving force of the heat exchanger (LMTD) decreases, decreasing the rate of heat transfer between combustion gases and water, and, hence, reducing the gas burner efficiency. This efficiency reduction trend was expected and agrees with the trends cited in literature. For the same range of tank water

temperature, similar efficiency reduction trends were reported by Maguire [19] and Makaire and Ngendakumana [20]. Other studies [18,29] reported the similar behavior for condensing gas boilers in terms of return water temperature, and have suggested reducing the return water temperature to below 54 °C to achieve more favorable performance.

4.3.Combined Solar and Natural Gas

In the hybrid mode of heating, tank water initially at 20±0.2 °C was heated to 60±0.2 °C using both solar and natural gas energy, simultaneously. Four different solar radiation values representative of typical summer weather conditions in Corvallis, Oregon, USA were used to analyze the performance of the hybrid solar/gas heating system. They consisted of heavily clouded sky (8/24/2017, 11:37 to 13:34), overcast sky (8/16/2017, 15:57 to 16:49), clear sky (8/17/2017, 13:04 to 13:54), and intermittent cloud covered sky (8/14/2017, 13:30 to 14:05).

The solar radiation measurements during the tests were 489±10 W m^{-2} on the heavily clouded day, 616±10 W m^{-2} on the overcast day, 973±10 W m^{-2} on the clear sky day, and 787±10 W m^{-2} on the intermittent cloud covered day. Figure 6 shows the solar fraction and natural gas contribution at these solar radiation values. It is seen that with increasing solar radiation, a larger solar fraction is achieved, and, hence, less natural gas energy is required.

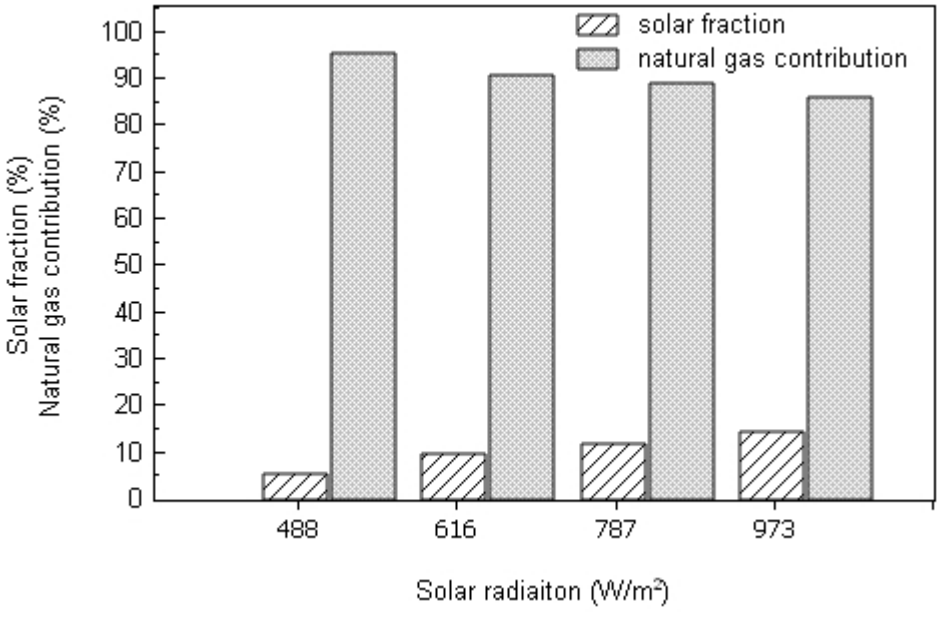

Figure 6: Solar fraction at different solar radiation values

However, as the solar fraction increases, and the energy contributed by natural gas decreases, the efficiency of the gas burner also decreases. This occurs in the hybrid heating mode because the temperature of water in the tank increases due to the partial heating provided by the solar input. As a result, the temperature driving force, LMTD, for the gas burner becomes is reduced and the rate of heat exchange between the combustion gases and tank water decreases. The overall efficiency of the gas burner at different solar fraction values is shown in Figure 7. Based on the higher heating value of natural gas, the efficiency of the gas burner was found to be 69.08, 66.80, 66.17, and 65.18% at solar fractions of 4.93, 9.40, 11.39, and 14.27%, respectively.

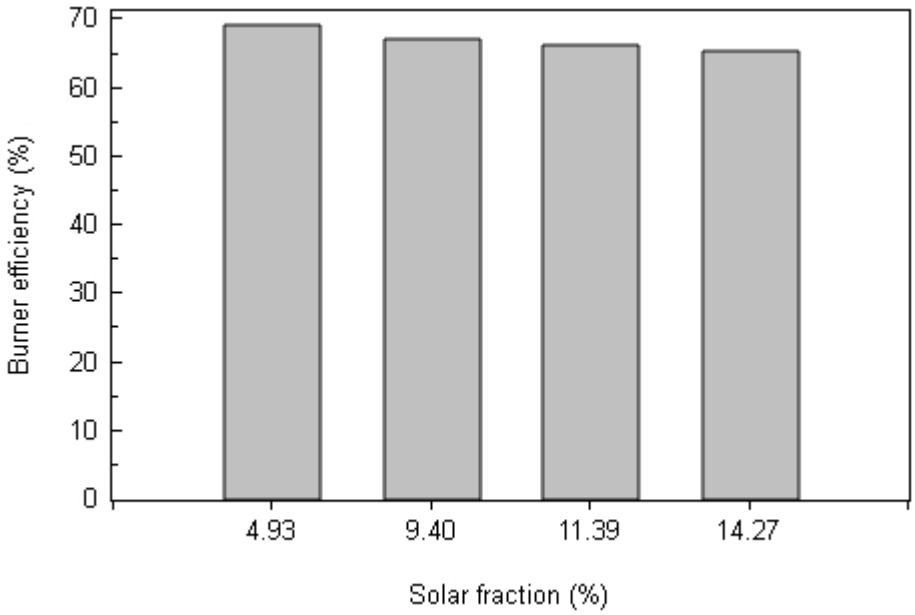

Figure 7: Gas burner efficiency at different solar fraction values

This set of experiments was conducted using the baseline control strategy of the commercial system where both natural gas and solar were used together to minimize tank heating time. In a real application, one may institute more sophisticated controls to use solar energy to heat the tank to as high a temperature as possible, and then use gas to accomplish the final lift, increasing the solar fraction. However, even using this control strategy would result in a lower burner efficiency due to the decreased LMTD. This differs from a standard solar/electric heating hybrid, as noted above, where the auxiliary heating efficiency is relatively insensitive to tank water temperature.

5. Potential Improvements of the Hybrid System

According to ASHRAE handbook [30], the annual domestic 60 °C hot water demand of a typical US family is 86,140 liters. Using the burner efficiency values obtained through this experimental research, the volume of natural gas consumed by the solar/gas hybrid system to satisfy this hot water demand for varying initial tank temperatures and solar fractions was approximated. Three inlet tank water temperature (20, 30, and 51.5°C) scenarios were considered. The final water temperature was assumed to be 60°C. For each inlet temperature, five different solar fractions (0, 25, 50, 75, and 100%) were assumed and the volume of natural gas consumed at corresponding solar fraction was calculated as Eq. (9):

$$V_{gas} = (1 - f)\frac{mC_{p,w}(T_{ini} - T_{fin})}{\eta_{burner}(T) * HV} \quad (9)$$

Here, $\eta_{burner}(T)$ is the experimental burner efficiency as a function of the initial tank water temperature. Figure 8 shows the relationship between solar fraction and volume of gas consumed by the solar/gas hybrid system for all three inlet water temperature scenarios. It is seen that the slope of the gas consumption curve decreases with an increase in inlet water temperature. That is, the incremental gas savings with increasing solar fraction is lower for higher initial tank temperatures. This is due to the decrease in gas burner efficiency with increasing inlet water temperature, as discussed above.

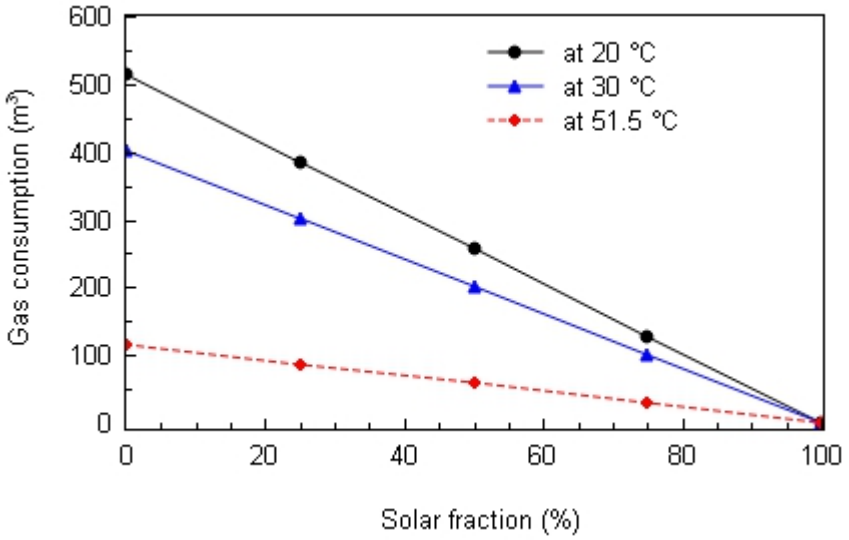

Figure 8: Approximate annual volume of natural gas consumed at three different initial water temperatures (all scenarios are for a final temperature of 60 °C).

The average volume of natural gas consumed by the hybrid system per degree of temperature rise is shown in Table 3. It is seen that for a higher initial tank water temperature, more natural gas is required per degree temperature rise. Hence, it is clear that lower inlet water temperature is desired to maximize gas burner efficiency and overall hybrid system efficiency.

Table 3: Natural gas consumption (m^3) per degree Celsius temperature rise

Solar fraction (%)	At 20 °C Burner efficiency of 69.23%	At 30 °C Burner efficiency of 66.43%	At 51.5 °C Burner efficiency of 65.50%
0	12.82	13.36	13.55
25	9.61	10.02	10.16
50	6.41	6.68	6.77
75	3.20	3.34	3.39
100	0.00	0.00	0.00

Based on the experimental study of the performance of the solar/gas hybrid system, there is clearly opportunity to explore new system configurations that maximize solar fraction while also maximizing efficiency of the gas auxiliary unit.

Under the current operational configuration of the hybrid system, the solar fraction can be maximized by using solar energy to heat the storage tank water to the required temperature, and when the solar input is not enough, the auxiliary gas burner would be turned on to top up the tank water temperature. However, as observed experimentally, the efficiency of the gas burner decreases at a higher starting water temperature. To avoid this inefficiency, it is suggested that instead of heating tank water that is pre-heated by solar input, the incoming cold water should be heated using an auxiliary gas burner and then mixed with heated water from solar storage tank on demand. This can be achieved by using a tankless gas-fired water heater and a thermostatic mixing valve as shown in Figure 9.

A storage gas water heater can be used as an alternative to an instantaneous burner. However, tankless water heaters have higher combustion efficiencies and eliminate standby losses that are common to storage water heaters [31].

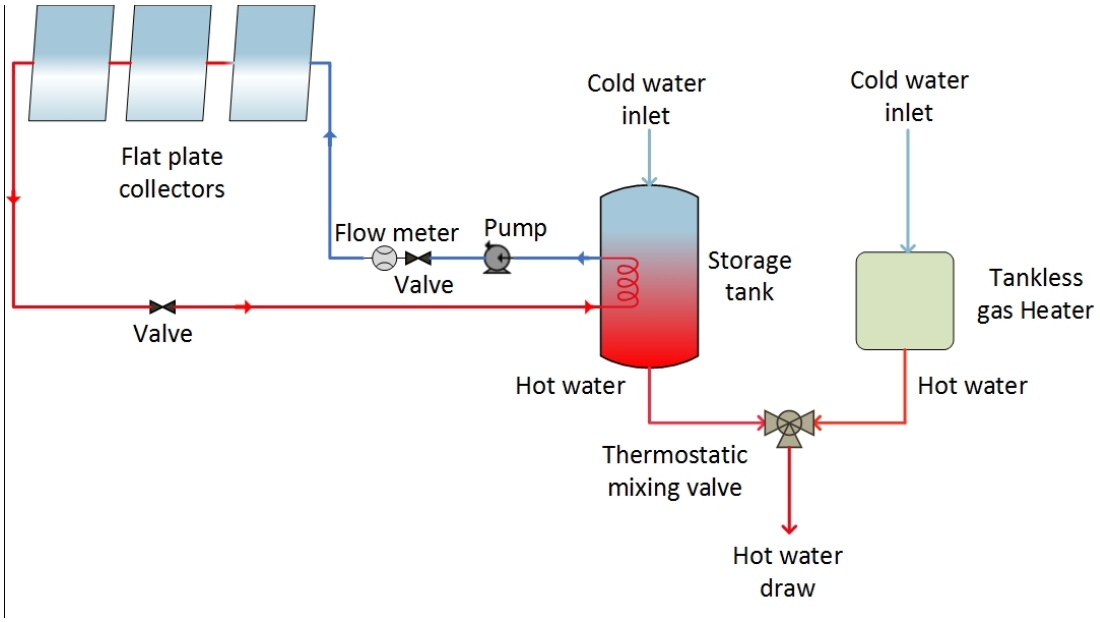

Figure 9: Alternative operation configuration

The operation of the thermostatic mixing valve can be controlled by using temperature sensors. A thermal-sensitive mechanism within the thermostatic mixing valve body automatically proportions the amount of hot water coming out of the solar heater and gas burner. The valve can be programmed such that when the temperature of the water exiting the solar tank falls below a minimum set point, the gas burner turns on to produce the required temperature blend. As observed experimentally, solar energy is usually enough to completely heat the tank to the required temperature during summer months. In contrast to this, solar fraction is typically low (0 to 25%) during winter months. So, a major proportion of hot water demand during winter would be provided by the gas heater. However, even with limited solar input, this control method still allows some solar input to be used in the winter months without degrading the gas burner efficiency, reducing total gas consumption.

The volume of natural gas consumed by the solar/gas hybrid system under the current and proposed configurations to satisfy annual hot water demand for a typical US family was calculated using Eq. (9) and shown in Figure 10. Two different gas burner types, a tankless, instantaneous gas burner and the existing storage type gas burner, were considered as two alternative proposed configurations. The tank inlet water temperature and the tank exit water temperature were assumed to be 20 and 60 °C, respectively. Five different solar fractions (0, 25, 50, 75, and 100%) were assumed. It is seen that less natural gas is consumed under the proposed configuration for both the

instantaneous and existing storage burner compared to the current configuration, particularly in low and midrange (0 to 25%) solar fractions, which is typical of winter or spring season operation. Under the proposed configurations, the gas burner is always heating incoming cold water, thus operating at maximum possible efficiency. So, unlike in the current configuration where the efficiency of gas burner decreases with increase in solar fraction, the efficiency of burner under proposed configuration remains constant regardless of changes in solar fraction. Natural gas savings offered by the proposed configuration with an instantaneous gas burner are higher than with existing gas burner because of its higher thermal efficiency [32].

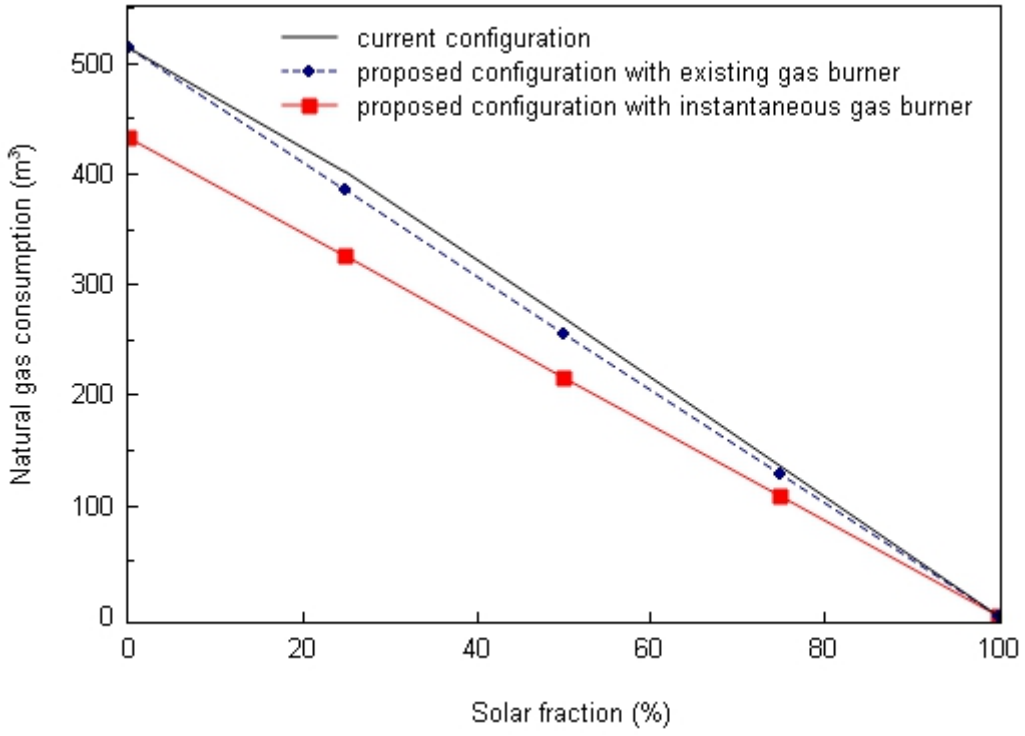

Figure 10: Approximate annual volume of natural gas consumed by the hybrid system under current and proposed configuration

The maximum difference in annual gas consumption between current configuration and proposed configuration with instantaneous gas burner in Figure 10 was obtained at solar fraction of 0% and found to be 80 m^3. This is approximately equivalent to 3240 MJ (30.68 therms) of energy in terms of HHV of natural gas. Similarly, the maximum difference in annual gas consumption between current configuration and proposed configuration with existing burner was obtained at solar fraction of 25% and found to be 16 m^3 which is equivalent to 665 MJ (6.3 therms) of energy in terms of HHV of natural gas.

The initial cost of an instantaneous gas-fired water heater is usually higher than a traditional storage water heater. Instantaneous water heaters typically last longer and have lower energy costs, which could justify its higher initial cost [33]. Although the annual energy savings offered by the proposed configuration for a single residence is relatively low, significant savings would be realized for multi-family residences or industrial process heating with much higher heat loads.

6. Conclusion

Performance of a solar/gas hybrid water heating system installed at Oregon State University in Corvallis, Oregon was monitored for a variety of typical weather conditions. Under different temperature lifts and solar insolation values, the hybrid system was operated at three different modes of heating: solar, gas, and combined solar/gas mode. Results showed that in the solar heating mode, the efficiency of the collector heating system was 41.97%, 39.82%, and 35.05% at initial tank water temperature of 20, 30, and 51.5 °C, respectively. For initial water temperatures of 20, 30, and 51.5 °C, the efficiency of the gas burner was found to be 69.2%, 66.4%, and 65.5% at the HHV and 76.7%, 73.6%, and 72.6% at the LHV of natural gas, respectively. In the combined solar/gas heating mode, the efficiency of the gas burner decreased with increasing solar fraction. For solar fractions of 4.93%, 9.40%, 11.39%, and 14.27%, the efficiency of the gas burner in terms of the HHV of natural gas was found to be of 69.08%, 66.80%, 66.17%, and 65.18%, respectively.

Results from the experimental study showed that energy consumed by the gas heating system per degree temperature rise of tank water increases with increase in inlet water temperature. So, instead of heating water that is pre-heated by solar energy, it is recommended that the cold incoming water be heated separately and mixed with the solar tank water using a thermostatic mixer. Doing so will result in natural gas energy savings when the solar/gas hybrid water heating system is operating at low and mid-range (15 to 50%) solar fraction, which is typical of spring and winter months. In addition to energy savings, the proposed configuration will also help to accurately quantify energy and cost savings offered by solar/gas hybrid system. This is because the efficiency of the gas heater will remain constant (corresponding to the inlet water temperature) regardless of the solar input, making the prediction of cost and energy savings a very straight forward problem. This configuration is very useful in evaluating cost and energy savings during a feasibility assessment of solar/gas hybrid water heating systems for residential and industrial applications. The results

from this study have been used by Karki [34] to develop design decision support tools to assess the feasibility of solar thermal energy systems for process heating applications.

7. Acknowledgments

Partial support of this work was provided by the U.S. Department of Energy, Office of Energy Efficiency and Renewable Energy, Advanced Manufacturing Office, under Award Number DE-EE0007701. The donation of solar thermal and gas-fired water heating equipment by NW Natural used in completion of this work is gratefully acknowledged.

Nomenclature

A_C	Collector aperture area (m^2)
c_P	Specific heat (J kg^{-1} K^{-1})
F_R	Collector heat removal factor
G_t	Solar irradiance (W m^{-2})
U_L	Collector overall heat transfer coefficient (W m^{-2} $°C^{-1}$)
T	Temperature (°C)
$\dot{m}$	Mass flow rate (kg s^{-1})
$\dot{Q}$	Rate of useful energy collected (J s^{-1})
V	Volume (m^3)
HV	Heating value (kJ m^{-3})
Q	Energy (J)
F	Solar fraction (%)
A	Area of heat exchanger (m^2)
U	Heat exchanger overall heat transfer coefficient (W $m^{-2}°C^{-1}$)
$LMTD$	Logarithmic mean temperature difference (°C)

Greek

η	Efficiency (%)
τ	Transmittance
α	Absorptance

Subscripts

u	Useful
i	Inlet
a	Ambient

g	Glycol
fi	Fluid inlet
fo	Fluid outlet
c	Collected
d	Delivered
s	System
burner	Natural gas burner
w	Water
ini	Initial
fin	Final
gas	Natural gas
solar	Solar heating system
auxiliary	Auxiliary heating system

References

[1] Residential Energy Consumption Survey (RECS) - Data - U.S. Energy Information Administration (EIA), (2015). https://www.eia.gov/consumption/residential/data/2015/.

[2] E.C. Balke, W.M. Healy, T. Ullah, An assessment of efficient water heating options for an all-electric single family residence in a mixed-humid climate, Energy Build. 133 (2016) 371–380. doi:10.1016/j.enbuild.2016.09.052.

[3] EIA, Table HC1.1 Fuels used and end uses in U.S. homes by housing unit type, 2015, (2015). https://www.eia.gov/consumption/residential/data/2015/hc/php/hc1.1.php (accessed April 1, 2018).

[4] J.A. Duffie, W.A. Beckman, Solar engineering of thermal processes, 4th ed., John Wiley & Sons, 2013.

[5] S.A. Kalogirou, Solar Energy Engineering: Processes and Systems, 2nd ed., Academic Press, 2013.

[6] CSN EN 12975-2 - Thermal solar systems and components - Solar collectors - Part 1: General requirements, (2006).

[7] S.J.B. Hale, ANSI/ASHRAE Standard 93-2003, Methods of Testing to Determine the Thermal Performance of Solar collectors, (2003).

[8] D. Rojas, J. Beermann, S.A. Klein, D.T. Reindl, Thermal performance testing of flat-plate collectors, Sol. Energy. 82 (2008) 746–757. doi:10.1016/j.solener.2008.02.001.

[9] K.R. Anderson, S. Hill, C. Selerberg, E. Guiterez, Experimental study of Sunearth flat plate solar collector, Int. J. Energy Eng. 4 (2014) 31.

[10] E. Zambolin, D. Del Col, Experimental analysis of thermal performance of flat plate and evacuated tube solar collectors in stationary standard and daily conditions, Sol. Energy. 84 (2010) 1382–1396. doi:10.1016/j.solener.2010.04.020.

[11] M.C. Rodríguez-Hidalgo, P.A. Rodríguez-Aumente, A. Lecuona, G.L. Gutiérrez-Urueta, R. Ventas, Flat plate thermal solar collector efficiency: Transient behavior under working conditions part II: Model application and design contributions, Appl. Therm. Eng. 31 (2011) 2385–2393. doi:10.1016/j.applthermaleng.2011.04.002.

[12] M.C. Rodríguez-Hidalgo, P.A. Rodríguez-Aumente, A. Lecuona, J. Nogueira, Instantaneous performance of solar collectors for domestic hot water, heating and cooling applications, Energy Build. 45 (2012) 152–160. doi:10.1016/j.enbuild.2011.10.060.

[13] I.M. Michaelides, P.C. Eleftheriou, An experimental investigation of the performance boundaries of a solar water heating system, Exp. Therm. Fluid Sci. 35 (2011) 1002–1009. doi:10.1016/j.expthermflusci.2011.02.001.

[14] L.M. Ayompe, A. Duffy, Analysis of the thermal performance of a solar water heating system with flat plate collectors in a temperate climate, Appl. Therm. Eng. 58 (2013) 447–454. doi:10.1016/j.applthermaleng.2013.04.062.

[15] Saving Energy with Electric Resistance Heating, National Renewable Energy Laboratory (NREL), Golden, CO, 1997. https://www.nrel.gov/docs/legosti/fy97/6987.pdf.

[16] Monthly Energy Review – March 2018, U.S. Energy Information Administration, 2018.

[17] B.M. Fronk, C.M. Keinath, Comparison of Primary Energy Consumption of Vapor and Non-Vapor Compression Natural Refrigerant Heat Pumps for Domestic Hot Water Applications, in: 12th IEA Heat Pump Conf. 2017, Rotterdam, Netherlands, 2017. http://hpc2017.org/wp-content/uploads/2017/05/O.1.7.2-Comparison-of-Primary-Energy-Consumption-of-Vapor.pdf.

[18] ASHRAE, 2016 ASHRAE Handbook: Heating, Ventilating, and Air-Conditioning Systems and Equipment (IP Edition), ASHRAE, Atlanta, GA, 2016.

[19] J.B. Maguire, A parametric analysis of residential water heaters, University of Colorado at Boulder, 2012. https://scholar.colorado.edu/mcen_gradetds/34.

[20] D. Makaire, P. Ngendakumana, Thermal performance of condensing boilers, in: 32nd TLM-IEA Energy Conserv. Emiss. Reduct. Combust., Nara, Japan, 2010. http://hdl.handle.net/2268/71592.

[21] S. Karki, K.R. Haapala, B.M. Fronk, Thermal Performance Evaluation of a Solar/Gas Hybrid Water Heating System, in: 5th Int. High Perform. Build. Conf. Purdue, West Lafayette, IN, USA, 2018.

[22] R. Aldrich, Indirect Solar Water Heating in Single-Family, Zero Energy Ready Homes, NREL (National Renewable Energy Laboratory (NREL), Golden, CO (United States)), 2016. https://www1.eere.energy.gov/buildings/publications/pdfs/building_america/65187.pdf.

[23] B.N. Taylor, C.E. Kuyatt, Guidelines for evaluating and expressing the uncertainty of NIST measurement results, US Department of Commerce, Technology Administration, National Institute of Standards and Technology Gaithersburg, MD, 1994.

[24] EES: Engineering Equation Solver | F-Chart Software : Engineering Software, (n.d.).

[25] S.A. Klein, W.A. Beckman, A general design method for closed-loop solar energy systems, Sol. Energy. 22 (1979) 269–282. doi:10.1016/0038-092X(79)90142-7.

[26] Y. You, E.J. Hu, A medium-temperature solar thermal power system and its efficiency optimisation, Appl. Therm. Eng. 22 (2002) 357–364. doi:10.1016/S1359-4311(01)00104-1.

[27] R. Celuppi, J. Scapinello, F.G.D. Andrade, J.H.P. Revello, J.D. Magro, Solar energy use for water pre-heating in boilers of agro-industries, Eng. Agrícola. 34 (2014) 451–460. doi:10.1590/S0100-69162014000300009.

[28] R.G. Boundy, S.W. Diegel, L.L. Wright, S.C. Davis, Biomass Energy Data Book: Edition 4, Oak Ridge National Laboratory (ORNL), Oak Ridge, TN (United States), 2011. doi:10.2172/1050890.

[29] D. Cutler, J. Dean, J. Acosta, D. Jones, Condensing Boilers Evaluation: Retrofit and New Construction Applications, National Renewable Energy Laboratory (NREL), Golden, CO, 2014. https://www.nrel.gov/docs/fy14osti/56402.pdf.

[30] ASHRAE, 2011 ASHRAE Handbook: HVAC Applications, ASHRAE, Atlanta, GA, 2011.

[31] M.A. Hoeschele, D.A. Springer, Field and Laboratory Testing of Gas Tankless Water

Heater Performance, ASHRAE Trans. 114 (2008) 453–461.

[32] B. Healy, Water Heating Technologies and Ratings, National Institute of Standards and Technology, 2015. https://www.nist.gov/sites/default/files/documents/iaao/Healy.pdf (accessed January 3, 2018).

[33] US DOE, Tankless or Demand-Type Water Heaters, (n.d.). https://www.energy.gov/energysaver/water-heating/tankless-or-demand-type-water-heaters (accessed January 3, 2018).

[34] S. Karki, Enabling Feasibility Assessment of Solar Thermal Energy Systems for Industrial Process Heating Applications, Oregon State University, 2018. https://ir.library.oregonstate.edu/concern/graduate_thesis_or_dissertations/k643b6518.